2021 IEEE/RSJ International Conference on Intelligent Robots and Systems (IROS)
September 27 - October 1, 2021. Prague, Czech Republic

2021 IEEE/RSJ International Conference on Intelligent Robots and Systems (IROS) | 978-1-6654-1714-3/21/$31.00 ©2021 IEEE | DOI: 10.1109/IROS51168.2021.9636587

Designing Rotary Linkages for Polar Motions

Aravind Baskar[1], Chang Liu[1], Mark Plecnik[2]*, and Jonathan D. Hauenstein[3]

***Abstract*— Polar linkages have two degrees-of-freedom (DOF) where one input joint angle controls the length of a radial segment while another controls its angle. Considering a theoretical planar robot model, this mapping between joint angles to output motions can be shown to be energetically advantageous over the ubiquitous two-revolute linkage. Since a polar linkage's typical construction involves a moving prismatic joint, it is cumbersome to implement alongside rotary electromagnetic actuators offsetting any advantage. In this paper, we present a procedure for designing polar linkages using only revolute joints. The procedure starts with a pre-existing single DOF straight line linkage and then finds the dimensions of a three-link attachment to produce the second DOF. In the end, the straight line linkage actuates the polar length and the attachment actuates the polar angle. The design process is framed under optimization with an objective that is both polynomial and invariant to the number of discretization points. This enables the techniques of numerical continuation to efficiently find complete sets of minima. We demonstrate our procedure with an example in which multiple minima are found including the global minimum. This computed design solution is then fabricated in order to validate the designed kinematics.**

I. Introduction

A typical design for the leg mechanism of a planar robot model is to attach an RR (revolute-revolute) mechanism to the body of a robot and actuate it at each joint with two copies of the same motor. These motors control the motion and forces of an endpoint that interact with the environment to locomote the robot. With this set-up, the mapping between joint torques and Cartesian force output are well mixed. Considering that the presence of gravity raises the force and torque requirements in the vertical direction, this begs the question as to whether a more decoupled approach is in order. Analysis of force and velocity commands at various points in the RR mechanism's workspace indicates configurations where the first has large instant power requirements while the second motor's is small, as well as configurations where the first motor has small instant power requirements while the second motor's is large. If only the former or latter were true, then one of the two motors could be downsized to match its lower power regime, resulting in mass and energy savings. Instead, each motor needs to be capable of shouldering the energetic burden individually at different points in time. To make matters worse, force and velocity commands executed at certain points in the workspace require one of the actuators to perform negative work as illustrated in Section II. Other researchers additionally note that kinematic coupling between the RR mechanism's actuator and endpoint motions leads to negative work production [1], and adversely impacts the performance of speed and force control between vertical and horizontal directions [2, pg. 149].

An approximate coupling of actuator motions to Cartesian directions can be shown to have advantages in this regard. One implementation of this coupling is the usage of a polar leg, that is, to use a rotary actuator to radially point a prismatic actuator toward the ground. This approach is particularly effective when that prismatic actuator is a powerful pneumatic [2],[3],[4] or hydraulic cylinder [5]. However, implementations of a polar leg with rotary electromagnetic (EM) actuators are more scarce. The accessibility, cost, portability, power density, and ease of implementation of rotary EM actuators makes this point substantial [6]. The bow leg of Zeglin [7] involved a polar leg powered by servos, however, the design objectives included an unconventional thrust actuation scheme that does not coincide with the objectives of the current paper. It is worth noting that at least a few partially actuated polar leg designs exist [8],[9],[10]. However, their relation to this work is tangential because only one joint is actuated.

One factor inhibiting broader usage of EM powered polar legs is that current rotary to linear motion solutions are not well suited for impact loads and large accelerations. For example, rack & pinion assemblies and ball screws involve heavy parts that should change direction quickly and often. Another relevant solution is to indirectly drive a prismatic joint, such as with a slider-crank linkage [11]. This approach admits a rotary actuator but still incorporates the challenges that come with building a prismatic joint, i.e., tolerating substantial torque over an accurate, low friction sliding motion. Revolute linkage assemblies provide several solutions for the rotary to linear problem, and have greater potential to be lightweight and sustain large forces. Furthermore, with parallel linkages, all actuators may be fixed relative to the body to limit acceleration of their inertias. However, it is unclear how to take these existing solutions and piece them together into a two degree-of-freedom polar leg. In this paper, we present a design procedure for converting extant approximate straight line linkages into approximate polar leg mechanisms using only revolute joints.

The approach involves designing a three link add-on. The add-on is to be attached to the body frame at one end and

*This work was supported by the National Science Foundation Award No. CMMI-2041789.

[1]Aravind Baskar and Chang Liu are with the Department of Aerospace and Mechanical Engineering, University of Notre Dame, Indiana, 46556, USA abaskar@nd.edu, cliu23@nd.edu

[2]*Mark Plecnik (corresponding author) is an assistant professor with the Department of Aerospace and Mechanical Engineering, University of Notre Dame, Indiana, 46556, USA plecnikmark@nd.edu

[3]Jonathan D. Hauenstein is a professor with the Department of Applied and Computational Mathematics and Statistics, University of Notre Dame, Indiana, 46556, USA hauenstein@nd.edu

to the straight line generator at the other. The add-on should reproduce the straight line of the generator and, by actuating its angle, be able to change that line's orientation. In this way, the add-on controls the polar angle while the straight line generator controls polar length. To find the dimensions of the add-on, an optimization problem is formed. The objective is formed from the sum of squares of kinematic constraint quantities that should ideally evaluate to zero. The objective summation is long because its terms correspond to discretization points of designated target curves. But notably, we perform an algebraic elimination on these constraints beforehand to wipe out configuration dependent variables, leading to a polynomial objective whose structure is invariant to the number of discretization points. This makes the ensuing computation very tractable, especially in terms of the toolset of polynomial homotopy continuation. A numerical ab initio homotopy is executed onto the optimization problem, finding that no more than 1,253 stationary points can exist. Specifically, we use the method of random monodromy loops [12], [13]. A parameter homotopy [14] is then executed to find all stationary points for an example problem. Saddles are then filtered out and the remaining minima are analyzed. In the example, the global minimum is found from which we fabricate a kinematic model that is verified to produce an approximate polar workspace.

The structure of the paper is as follows. Section II performs a preliminary exercise to motivate the design of polar linkages by demonstrating their potential for energetic benefits. The formulation and numerical reduction of our design equations is contained in Section III. These results are applied to compute a polar linkage example in Section IV. In Section V, a kinematic model of one of the computed solutions is constructed and validated for its approximate polar workspace. Conclusions are offered in Section VI.

II. Motivation

To understand the advantages that a polar leg design might offer in terms of mechanical power flow, consider the three serial chains displayed in Fig. 1: (a) an RR chain, (b) a PP chain, and (c) an RP chain. The RR chain consists of two serially actuated revolute joints. The PP chain consists of two serial, orthogonal prismatic joints, each of which is actuated by a rotary actuator through some means. In Fig. 1b, this is conveyed by rack and pinions but, for the current exercise, how rotary to linear motion is achieved does not matter. The RP chain consists of a revolute joint that aims a prismatic joint in which the two joint axes intersect. Once again, a rotary-to-linear transformation sets up the leg to have two rotary actuators.

The motion inputs of each leg are marked as $(\theta_1, \theta_2)^\top$ For the RR and RP chains, θ_1 is measured from the downward vertical. For the RR chain, θ_2 is the relative angle between proximal and distal segments. The kinematic Jacobians of the three serial chains are

$$[J_{\text{RR}}] = \begin{bmatrix} l_1 \cos\theta_1 + l_2 \cos(\theta_1+\theta_2) & l_2 \cos(\theta_1+\theta_2) \\ l_1 \sin\theta_1 + l_2 \sin(\theta_1+\theta_2) & l_2 \sin(\theta_1+\theta_2) \end{bmatrix}, \quad (1)$$

$$[J_{\text{PP}}] = \begin{bmatrix} L_1 & 0 \\ 0 & L_2 \end{bmatrix}, \quad (2)$$

$$[J_{\text{RP}}] = L \begin{bmatrix} \theta_2 \cos\theta_1 & \sin\theta_1 \\ \theta_2 \sin\theta_1 & -\cos\theta_1 \end{bmatrix}, \quad (3)$$

where l_1 and l_2 are the segment lengths of the RR chain. L_1, L_2, and L are the radii of the pinions shown in Fig. 1. For this exercise, they will ultimately cancel out and so their actual values are inconsequential.

The Jacobian transforms velocities and forces/torques between the actuators and endpoint. Let's notate the motor velocities as $(\dot\theta_1,\, \dot\theta_2)^\top$, the endpoint velocity as $(v_x,\, v_y)^\top$, the motor torques as $(T_1,\, T_2)^\top$, and force applied at the endpoint as $(F_x,\, F_y)^\top$. The relevant transformations are

$$\begin{bmatrix} \dot\theta_1 \\ \dot\theta_2 \end{bmatrix} = [J_{xx}]^{-1} \begin{bmatrix} v_x \\ v_y \end{bmatrix}, \qquad \begin{bmatrix} T_1 \\ T_2 \end{bmatrix} = [J_{xx}]^T \begin{bmatrix} F_x \\ F_y \end{bmatrix}. \quad (4)$$

We note that inertial forces and losses have been neglected, and in doing so, suggest that the kinematic effects captured in Eqns. (4) are substantial enough to study on their own. With this formulation, it is easy to show that the power generated at the endpoint in an instant must equate to the motors' mechanical power output. The dot product of Eqns. (4) yields

$$\begin{bmatrix} T_1 & T_2 \end{bmatrix} \begin{bmatrix} \dot\theta_1 \\ \dot\theta_2 \end{bmatrix} = \begin{bmatrix} F_x & F_y \end{bmatrix} [J][J]^{-1} \begin{bmatrix} v_x \\ v_y \end{bmatrix}. \quad (5)$$

However, Eqn. (5) fails to capture the role that the Jacobian plays in distributing power. Given the force and velocity of the endpoint, and the current configuration of the mechanism, the kinematic Jacobian dictates how instantaneous commanded power P_{kin} is distributed between the motors. This is found simply by evaluating the right sides of Eqns. (4), then computing $P_1 = T_1\dot\theta_1$ and $P_2 = T_2\dot\theta_2$. Note that although $P_{\text{kin}} = P_1 + P_2$, there is no guarantee that both P_1 and P_2 will be positive. If P_1 happens to be negative, then P_2 must be greater than P_{kin}. In other words, the mechanical power output by one of the motors must be greater than the mechanical power of the commanded task. Moreover,

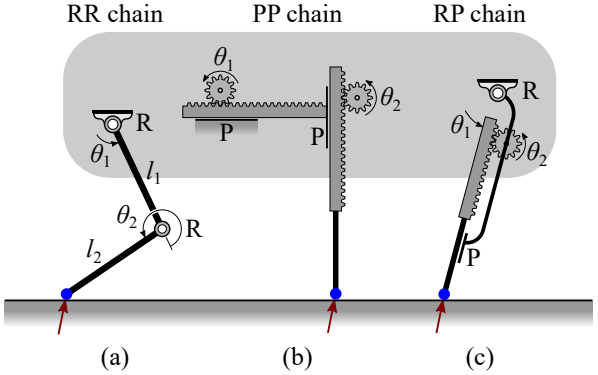

Fig. 1: Serial two DOF chains: (a) an RR chain, (b) a PP chain, and (c) an RP chain. Power distributions of these three chains were calculated for characteristic force/velocity commands at various points in their workspaces.

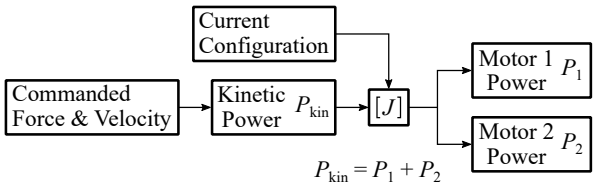

Fig. 2: Neglecting losses, an instantaneous force/velocity command specifies a kinetic power which distributes between actuated joints as defined solely by the kinematic Jacobian. P_1 or P_2 may be negative although P_{kin} is positive.

this is all due to kinematics, before Joule heating, friction, compliance, and all other losses are accounted for.

To see this and other behaviors, we perform a brief study. Consider the limb commanded to perform a vigorous task of accelerating upwards at four G's and forwards at one G. The commanded force would be $\mathbf{F} = mg(1,5)^\top$ (minding the offset of the robot's weight itself). And consider a commanded velocity collinear to $\mathbf{F}$ such that the robot bounds to a height h, i.e., $\mathbf{v} = \frac{1}{5}\sqrt{2gh}(1,5)^\top$. We observe the power distribution between actuators for each of the serial chains of Fig. 1 at various points in the workspace.

We note that the ratio P_1:P_2 is defined only by the directions of $\mathbf{F}$ and $\mathbf{v}$. With respect to this ratio, their magnitudes cancel out as can be seen in the power balance of Eqn. (5). In this sense, the magnitudes defined above are superficial except to illustrate this study with realistic values. To this end, we proceed forward with additional values $m = 1\,\text{kg}$, $h = 0.5\,\text{m}$, and $l_1 = l_2 = 0.15\,\text{m}$. The commanded kinetic power is $P_{kin} \approx 160\,\text{W}$. The results are given in Fig. 3 and Table I.

The power distribution was computed at six points in the workspace, marked A–F in Fig. 3, for all three serial chains. Table I displays the data that corresponds to each of these points. This table includes the instantaneous power values at each motor necessary to complete the commanded motion, as well as the ratio of P_1 to the total requested power P_{kin}. To understand this latter value, we note that at point A, the θ_1 motor of the RP chain would provide 7% of the necessary energy meaning the θ_2 motor must provide the remaining 93%. Considering the RR chain at point A, the θ_1 motor would provide -21% of the energy meaning that it is doing negative work at that instant. Therefore, the θ_2 motor must provide 121% of the requested kinetic power at that instant.

It can be unintuitive that a net positive power kinematically requires a negative power component. The condition for this to occur is simply that the commanded torque and velocity at an actuated joint oppose each other. One such configuration is given in Fig. 3. For the endpoint to move in the direction of $\mathbf{v}$, the θ_1 joint must rotate clockwise. For the endpoint to exert a force in the direction of $\mathbf{F}$, it must resist the opposite of $\mathbf{F}$. Consider the moment arm of $-\mathbf{F}$ from the fixed pivot in Fig. 3, it is clear that a counterclockwise torque must be exerted by the motor.

The preceding study is brief. Combinations of configurations and force/velocity specifications that necessitate

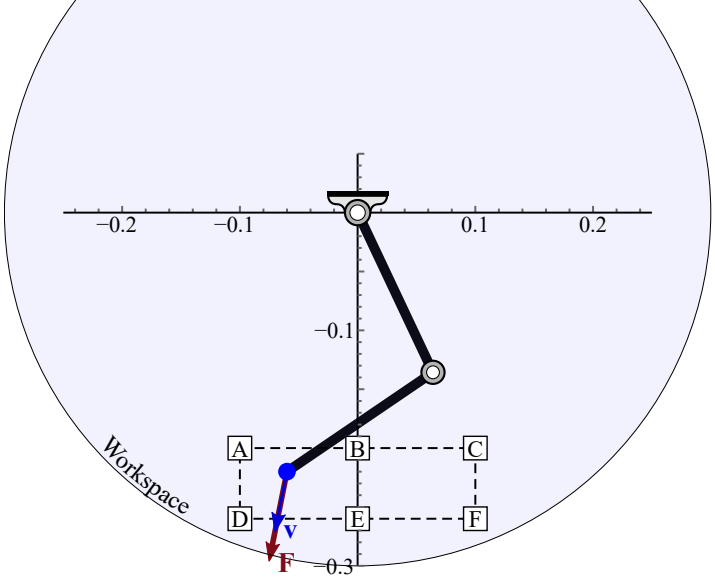

Fig. 3: The three serial chains of Fig. 1 were evaluated at six points in their workspaces to determine instantaneous power distribution between actuators for a characteristic force/velocity command. Pictured above is only the RR chain. Corresponding values at points A-F are given in Table I.

TABLE I: The results of a preliminary exercise comparing the three serial chains shown in Fig. 1 according to their power distributions between actuators during a characteristic force/velocity command at the workspace points A-F shown in Fig. 3.

	P_1 (W)	P_2 (W)	$\frac{P_1}{P_{kin}}$ (%)	P_1 (W)	P_2 (W)	$\frac{P_1}{P_{kin}}$ (%)	P_1 (W)	P_2 (W)	$\frac{P_1}{P_{kin}}$ (%)
	A			**B**			**C**		
RR	−34	194	−21	34	126	21	147	13	92
PP	6	154	4	6	154	4	6	154	4
RP	11	149	7	6	154	4	60	100	38
	D			**E**			**F**		
RR	−62	222	−39	60	100	37	226	−67	142
PP	6	154	4	6	154	4	6	154	4
RP	5	155	3	6	154	4	46	114	29

negative power can be found for all three of the serial chains. Rather than exploring all combinations, we suggest that the combinations depicted in Fig. 3 are representative in order to make design decisions. In particular, we point out the relatively low values of P_1/P_{kin} for the PP and RP chains shown in Table I. This indicates that these chains might benefit from asymmetric motor specification. The θ_1 motor can operate in a lower power regime than the θ_2 motor. Intuitively, for these two chains, the θ_1 motor predominantly controls horizontal Cartesian velocities while the θ_2 motor is predominantly resisting gravity in the vertical direction. However, since both of these chains contain a P joint, their integration with electric motors is challenging.

Rotary-to-linear solutions are heavy and torque limited (rack & pinion, ball screws). Linkage designs that convert rotary to linear motions exist, but their required positioning of links makes it unclear how these might be converted into two degree-of-freedom leg mechanisms. To address this problem, we focus on a design technique to create linkages with a map of $(\theta_1, \theta_2)^\top$ to endpoint coordinates that liken to an RP chain with the critical exception that we create parallel chains rather serial. This allows both actuators to remain fixed to the robot body, minimizing large accelerations of

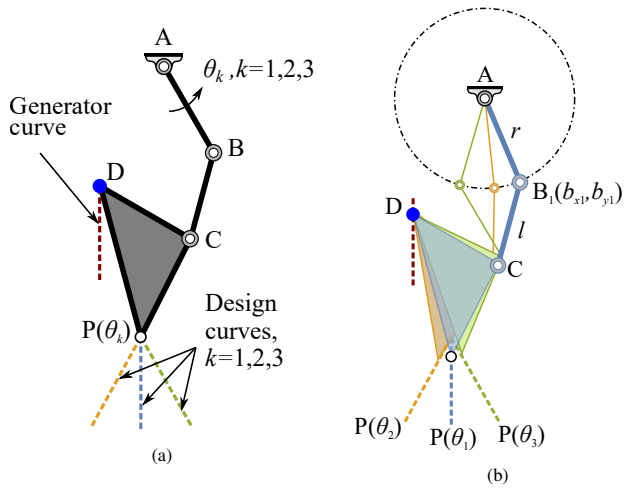

Fig. 4: Schematic of the design of a 3R mechanism.

their inertias.

III. Design Formulation

To begin our design formulation, we assume that an approximate straight line generator is already in hand. Examples of these sorts of linkages can be found in [15]. The objective is to design additional links to attach to this generator in order to displace its line to a convenient location and allow the ability to reorient this line as controlled by an actuator placed at the base link of the add-on. In tandem with an actuator placed on the generator itself, the two would serve to actuate and orient this line of action, thus instantiating a polar workspace. The add-on mechanism consists of three links connected from the base to the straight line generator by three revolute joints, and so is referred to as a 3R linkage. Such a set up is shown in Fig. 4a where the three revolutes are labeled as A, B, and C, and the connection point to the straight line is labeled D. The endpoint is labeled P, and should produce at least approximate polar motions as parameterized by the base angle θ and motions along the straight line.

A. Mathematical Model

Consider three sets of approximate straight lines (referred to as curves hereon) as design requirements at P. Note that these curves are to be functions of the polar angle input θ_k, $k = 1, 2, 3$, respectively, whose values are to be determined. While a continuous association with the polar angle is preferred, we pick three sets of design curves over the desired range to simplify the model. This allows us to initiate vector loop equations starting from B_k, $k = 1, 2, 3$, instead of A. Once the points B_k, $k = 1, 2, 3$, are determined, the point A can be obtained by fitting a circle through the points B_k and locating its center as summarized in Fig 4b.

We fixed the parameter length DP and solved the PR inverse kinematic problem to determine the orientation ψ_{kj} of the vector DP for the three set of curves through all of the design positions, which are discrete points on the generator curve at D_j, $j = 1, 2, ..., N$. The vector CD is denoted using the variables $(q_x, q_y)^\top$ in an initial configuration. The vector loop equation associated with each design position can be written as follows:

$$(b_{xk}, b_{yk})^\top + l(\cos(\phi_{kj}), \sin(\phi_{kj}))^\top + \mathbf{R}[\psi_{kj}] \cdot (q_x, q_y)^\top = (d_{xj}, d_{yj})^\top. \quad (6)$$

Here, $\mathbf{R}$ represents the 2D rotation matrix and ϕ_{kj} is the rotation angle associated with the binary link BC at a design position. Eliminating ϕ_{kj} can be performed by considering the rigidity of the link BC as follows:

$$\eta_{kj} := l^2 - ||(d_{xj}, d_{yj})^\top - \mathbf{R}[\psi_{kj}] \cdot (q_x, q_y)^\top - (b_{xk}, b_{yk})^\top||^2 = 0. \quad (7)$$

A further simplification is made by replacing l^2 with l_s to reduce the algebraic degree of the system. Thus, the nine variables in the above equation are

$$\mathbf{d} = \{b_{x1}, b_{y1}, b_{x2}, b_{y2}, b_{x3}, b_{y3}, l_s, q_x, q_y\}.$$

Hence, if the design positions are to be met exactly, only specifying nine design positions in total are possible. However, for a larger number of design positions in each of the three sets, one can replace exact specifications with an optimization problem where the residual in the equation η_{kj} is minimized over all the design positions. Accordingly, the objective of the optimization is a sum of squares of the residual over all the design positions, namely

$$f = \frac{1}{2} \sum_{k=1}^{3} \sum_{j=1}^{N} \eta_{kj}^2. \quad (8)$$

This error measure has been used previously in literature for kinematic synthesis to successful effect, e.g. [16]. The first order necessary conditions of optimality are:

$$f_{\mathbf{d}} = \sum_{k=1}^{3} \sum_{j=1}^{N} \eta_{kj} \frac{\partial \eta_{kj}}{\partial \mathbf{d}} = \mathbf{0}. \quad (9)$$

This leads to a system of nine polynomial equations in nine variables whose roots are the stationary points of the unconstrained optimization problem. Polynomial systems such as this one are nonlinear in nature and admit a large number of solutions termed as the *root count* of the system. The root count can be bounded based on the monomial structure of the polynomials, called the *BKK bound*, e.g., see [17, § 8.5]. It is important to note that Eqn. 9 is devoid of configuration dependent variables generated from the discretization. It does contain configuration dependent input specifications from the discretization, but these parameters do not alter its monomial structure. This means that the root count of this system does not change as the number of discretization points increases. This allows us to use the technique of numerical continuation to solve a generic polynomial system of the same structure and solve any subsequent problems using the solutions of the generic system. The former step is called the *ab initio* step and the later step is called the *parameter homotopy* step [18].

B. Numerical Reduction

There are several approaches to compute the root count and complete the ab initio step. One approach is to bound the root count and employ a single homotopy. For example, an elementary analysis shows the multi-homogeneous Bézout number [19] of Eqn. 9 is 203,877, which is an upper limit on the root count. Another bound on the root count is the BKK bound, which was found to be 6,561 [20]. Thus, one can employ a multi-homogeneous or a polyhedral homotopy tracking 203,877 or 6,561 paths, respectively, to complete the ab initio step.

Rather than use a single homotopy, another approach is based on building up to a complete solution set using a sequence of homotopies. The technique of random monodromy loops (RML) [12], [13] uses a series of homotopy loops that start and end at the same system while taking different paths. By starting from a seed solution, roots are accumulated iteratively with statistical approximations of the root count computed after each iteration [12]. Several techniques can be employed for a stopping criterion, e.g., comparing the actual number of roots collected with a statistical approximation of the root count, stopping after several iterations yielding no new roots [21], or employing a trace test to validate that all roots have been found [12], [22].

For computational efficiency, the choice of method depends upon the expected order of magnitude difference from the multi-homogeneous Bézout number and the actual root count, the computational cost of computing the BKK bound together with its expected order of magnitude difference with the actual root count, and the cost of performing many random monodromy loops. If an upper bound is expected to be comparable to the root count, a single homotopy is often preferred. When the difference is expected to be large, the probabilistic approach of RML can be more efficient.

For the ab initio setup, a generic design problem with randomly chosen values for d_{xj}, d_{yj}, and ψ_{kj}, $k = 1, 2, 3$, $j = 1, 2, ..., 7$ is created. Based on the expected difference between the upper bounds and the actual root count, our computation utilized RML via the software `Bertini` [18], [23] running on an Intel Xeon 2.30 GHz system with 192 parallel cores in the Center for Research Computing at the University of Notre Dame. Refer to [13] for more information on the details of the numerical technique. In about three minutes of real computational time, this showed that the root count of this polynomial system was 1,253. This result was independently verified in [24]. This means that the objective displayed in Eqn. 8 can have no more than 1,253 stationary points which can be found, both real and complex, by tracking a 1,253 path parameter homotopy in about 28 seconds on the computational resources listed above.

IV. Example Polar Linkage

The optimization framework described in Section III was applied to an example design of a polar linkage. The approximate straight line generator used was a six-bar linkage designed independently of this work, depicted in Fig. 5. The objective is to find a 3R linkage add-on that regenerates the approximate straight line below the pre-existing pivot points and provides an additional degree of freedom to reorient the regenerated line resulting in a polar workspace. The length of DP was chosen as $0.06\,\mathrm{m}$ (refer to the inset), roughly setting the downward translation of the polar workspace. The shaded region in the figure shows the bottom half area of the reachable points by P for this choice. The design curves specified must be restricted to this region. For this set of design curves, the desired orientation of the vector DP can be determined by solving for the inverse kinematics which is elementary in this case. For enabling this, the generator curve is represented as 440 discrete points. For every point $D_j,\ j = 1, 2, ..., 440$ in the generator curve, the angular orientation of DP corresponding to each of the three design curves is computed to serve as the specification for the optimization problem.

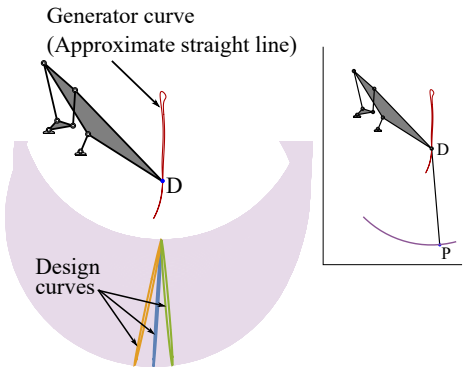

Fig. 5: Specification of design curves for the optimal design of a polar leg linkage.

A homotopy is constructed from the previously solved ab initio system to the target system corresponding to the practical example. The start solutions of the ab initio system, 1,253 in number, are tracked onto the target system in the `Bertini` software in under 30 s with the same resources as above. The number of successful paths for this numerical example was 1120, about 90% of paths. In traditional predictor-corrector homotopy path tracking, e.g., see [25], [26], Newton's method is used as the correction step which often hits the limit of numerical precision when confronted with an ill-conditioned Jacobian. Here, we employed double precision tracking to balance between efficiency and robustness. Of the successful paths, only 12 corresponded to physical solutions with real values for the link dimensions, which are listed in Table II. Five of the 12 are local minima, while the rest are saddle points. Only three of the 12 candidates, which are labeled #3, #8, and #9, were singularity-free, making them viable. Candidate #9, even though a minimum, returned a poor approximation of the desired curves as can be inferred from the value of the objective function when compared against #3 and #8. Candidates #3 and #8 trace the design curves fairly well for various values of the 3R base joint input as shown in Figs. 6 and 7, respectively. Design #3 is undesirable since all pivots do not remain above the polar workspace. Design #8, which is incidentally the global

TABLE II: Stationary points of the optimization.

#	Design parameters (mm)									Type	Obj. f $\times 10^{-4}$
	b_{x1}	b_{y1}	b_{x2}	b_{y2}	b_{x3}	b_{y3}	l	q_x	q_y		
1	−43.178	−22.658	−43.415	−22.679	34.133	−24.103	42.029	−15.005	8.891	Min.	0.3129
2	−31.137	−70.126	−19.840	−71.631	−13.376	−70.052	18.688	3.518	55.227	Saddle	0.3318
3	17.795	−163.628	3.356	−182.959	24.366	−143.559	64.843	23.416	142.118	Min.†	0.1934
4	−20.548	−70.860	−23.773	−70.849	−17.090	−70.483	17.390	2.663	55.365	Saddle	0.3320
5	−12.890	−10.275	−25.654	−9.983	−26.552	−9.529	18.754	−2.039	−5.312	Saddle	0.3231
6	15.631	−18.146	−46.649	−15.906	−46.668	−15.610	35.633	−4.395	1.608	Min.	0.3147
7	−19.670	−5.321	−2.311	−6.374	−20.829	−4.478	19.658	−10.118	−9.679	Saddle	0.3217
8	−75.247	30.456	−72.298	23.736	−77.389	37.014	61.802	−3.535	−44.795	Min.* †	0.1583
9	1.809	−98.362	−3.973	−103.388	−50.927	−100.136	33.690	6.624	80.925	Min.†	0.3309
10	−12.523	−75.408	−32.275	−72.952	−8.902	−73.991	19.154	0.638	59.540	Saddle	0.3323
11	−36.811	−8.322	−36.875	−8.053	−21.630	−9.503	19.246	7.582	−6.730	Saddle	0.3223
12	−16.252	−76.668	−19.917	−77.559	−30.819	−76.970	19.511	5.206	60.726	Saddle	0.3325

∗ Global minimum.
† Singularity-free 3R mechanism.

TABLE III: Power distributions between actuators during a characteristic force/velocity command at the workspace points A-F shown in Fig. 8.

	P_1 (W)	P_2 (W)	$\frac{P_1}{P_{\text{kin}}}$ (%)	P_1 (W)	P_2 (W)	$\frac{P_1}{P_{\text{kin}}}$ (%)	P_1 (W)	P_2 (W)	$\frac{P_1}{P_{\text{kin}}}$ (%)
	A			**B**			**C**		
#8	40	120	25	−0.6	160	−0.4	64	95	40
	D			**E**			**F**		
#8	1.4	158	1	0.8	159	0.5	52	107	33

minimum, shows positive ground clearance, hence a natural choice for building a physical robotic system based on its specifications. In Fig. 7, two additional curves generated by the mechanism are shown along with the ones corresponding to the three design specifications to indicate the range over which the straight line approximation holds.

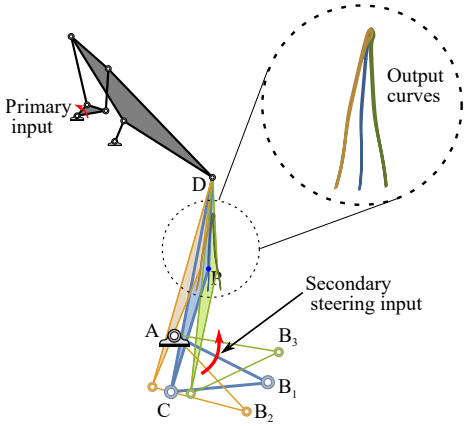

Fig. 6: An optimal design candidate #3 for the design of a polar leg linkage. The output curves are singularity-free. However, the mechanism has negative ground clearance, making it undesirable.

V. Prototype

As a condition for achieving the energetic advantages presented in Section II, we analyze the instantaneous power distribution between the actuators of design #8. To repeat the takeaway of Section II concisely: the behavior we desire

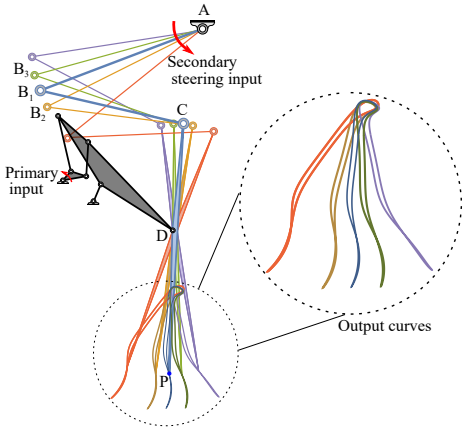

Fig. 7: Global design candidate #8 for the optimization problem. The mechanism is a suitable one as it is singularity-free with sufficient ground clearance.

is an instantaneous asymmetric power distribution between joint angles given characteristic velocities and loading at the endpoint at various places in the workspace. This distribution should minimize the power requested at one joint, without going negative, and maximize the power requested at the other. Fig. 8 and Table III summarizes this analysis and all the relevant parameters are found to be in order. When compared with the three cases RR, PP, RP chains, the design presented in Fig. 8 produces desirable power characteristics similar to the RP chain without using prismatic joints. As a further illustration of this behavior, we use kinematic accuracy as a surrogate measurement. The factors defining power requests at each input joint are not purely kinematic in nature, but we believe kinematics play a dominant role.

A kinematic model of design solution #8 (Fig. 7) was constructed to validate that it achieves at least an approximate polar motion. This exercise demonstrates that the dimensional sensitivity and tolerancing required of design #8 fall within the capabilities of conventional fabrication techniques. The approximate straight line generator was cut out of 6061 aluminum by a CNC mill, see Fig. 9. The 3R linkage add-on was 3D printed with PLA. Joints

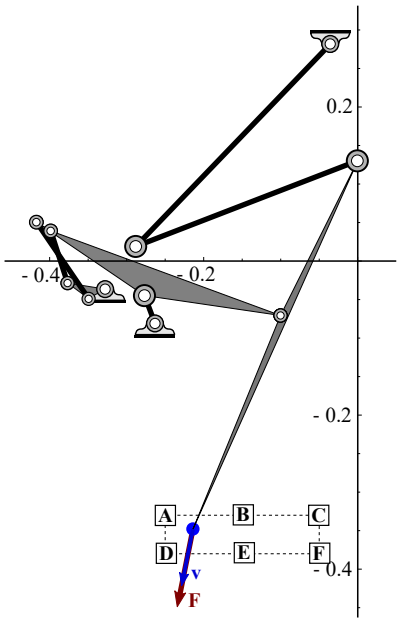

Fig. 8: Instantaneous power distribution between actuators for a characteristic force/velocity command for the Design #8 shown in Fig. 7. Corresponding values at points A-F are given in Table III.

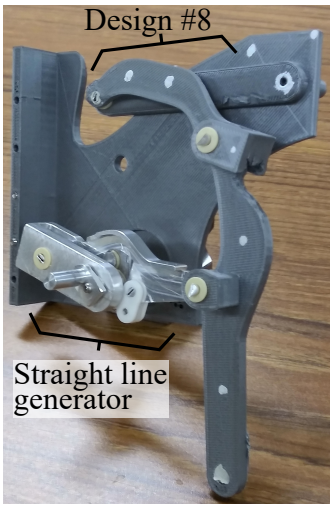

Fig. 9: A view of the partially assembled kinematic model.

were accommodated with a mix of plastic bushings and ball bearings. The kinematic model was video recorded and processed [27] to test its kinematic accuracy. Since one half of the generator curve possessed smoother transmission characteristics than the other, the smoother half was used for the recordings. The generator curve and approximate polar motion are shown in Fig. 10. The curves marked I-V correspond to motions produced when the 3R input joint is held fixed at various angles. Our metric of merit is the straightness of these radiating curves. To assess this for a single curve, temporal data points from the video recordings were resampled to be made spatially uniform. This was accomplished by interpolating splines through data points, then choosing new spatially uniform data points from those splines. A line was fitted through the resampled points and a raw error metric e was computed as the average distance of data points from this line. Then, all data points were projected onto the line and the two extremes were used to bound the line into a segment. The length of the segment, Γ, was then used to normalize error into a percentage, $\hat{e} = e/\Gamma$. The angle of the line segment was used to describe the rough angle of each curve. Over the five recorded curves, radial polar straight lines deviated from the ideal by an average error of 2.17%.

VI. Conclusion

This work described a procedure for designing polar linkages in the absence of prismatic joints. This is accomplished by transforming pre-existing single DOF straight line generators into two DOF polar linkages. The procedure begins with an approximate straight line generator curve, forming one of the two DOF. A 3R serial link structure should attach to the generator curve to form a closed chain. The terminal link of the 3R is required to trace a series of approximate straight lines while holding its proximal link fixed in order to approximate the radial movements of a polar workspace. The design challenge is to find 3R dimensions that actually accomplish this, which was solved by forming an optimization problem and applying numerical homotopy continuation to compute critical points. To form the objective, kinematic loop equations are formed over n design configurations corresponding to discretized versions of the desired curves. These equations introduce hundreds of configuration dependent unknowns, making any ensuing optimization intractable. Instead, all configuration dependent variables are algebraically eliminated so that the objective is formed by treating kinematic constraints as quantities rather than equalities, and summing their squares. The resulting objective is polynomial and its monomial structure is invariant to the number of discretization points. This is a nice advantage because it enables homotopy continuation to numerically reduce the problem once and those results are applicable to any discretization using a technique called parameter homotopy. This has a large positive effect on both computational efficiency and completeness of the resulting optimization. Our technique can find nearly all minima of this objective in less than 30 seconds. We demonstrate the importance of finding all minima through a numerical example to design a polar robot leg. In this example, we found five minima including the global minimum. The global minimum design is found to be sufficiently practical and subsequent fabrication demonstrated kinematic accuracy.

We are motivated to design polar linkages since, when used as robotic legs, they can be shown to demonstrate energetic advantages. In particular, polar linkages do a better job than RR linkages distributing requested instantaneous power between actuated joints for common motion and loading scenarios of legged robots. The power distribution sought is for one joint to shoulder the energetic burden while the other joint's role is energetically minimal and does not generate negative power. This is advantageous as only one

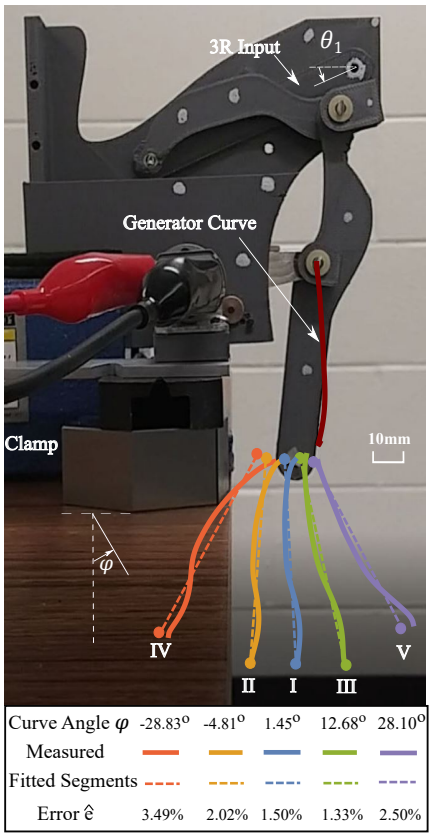

Fig. 10: A compilation of curves traced during video recordings of the kinematic model.

motor needs to be sized for large power output. Note that the typical RR mechanism requires each motor to shoulder nearly the entire energetic output by itself at different points in its workspace meaning that both motors need to be sufficiently powerful. Moreover, our design procedure leads to polar two DOF mechanisms absent of prismatic joints. The motivation to circumvent prismatic joints is due to the general cumbersome nature of their implementation with rotary EM actuators.

ACKNOWLEDGMENT

All authors gratefully acknowledge the support of the National Science Foundation Award No. CMMI-2041789.

REFERENCES

[1] S. Hirose, Y. Fukuda, K. Yoneda, A. Nagakubo, H. Tsukagoshi, K. Arikawa, G. Endo, T. Doi, and R. Hodoshima, "Quadruped walking robots at Tokyo Institute of Technology," *IEEE Robotics Automation Magazine*, vol. 16, no. 2, pp. 104–114, Jun. 2009.

[2] H. B. Brown and W. Lee, "Articulated Leg," in *Dynamically Stable Legged Locomotion*. Cambridge, MA: Massachusetts Institute of Technology, 1989, vol. LL-6, pp. 147–181.

[3] M. H. Raibert and J. K. Hodgins, "Animation of dynamic legged locomotion," in *Proceedings of the 18th Annual Conference on Computer Graphics and Interactive Techniques*, ser. SIGGRAPH '91. New York, NY, USA: Association for Computing Machinery, Jul. 1991, pp. 349–358.

[4] M. H. Raibert, *Legged Robots That Balance*. Cambridge, MA: The MIT Press, 1986.

[5] X. Chen, F. Gao, C. Qi, X. Tian, and J. Zhang, "Spring Parameters Design for the New Hydraulic Actuated Quadruped Robot," *Journal of Mechanisms and Robotics*, vol. 6, no. 021003, Jan. 2014.

[6] J. M. Hollerbach, I. W. Hunter, and J. Ballantyne, "A Comparative Analysis of Actuator Technologies for Robotics," in *The Robotics Review 2*. Cambridge, MA: MIT Press, 1992, pp. 299–342.

[7] G. Zeglin, "The Bow Leg Hopping Robot," Ph.D. dissertation, Carnegie Mellon University, Pittsburgh, Pennsylvania, 1999.

[8] J. E. Clark and M. R. Cutkosky, "The Effect of Leg Specialization in a Biomimetic Hexapedal Running Robot," *Journal of Dynamic Systems, Measurement, and Control*, vol. 128, no. 1, pp. 26–35, Dec. 2005.

[9] M. Buehler, "Dynamic Locomotion with One, Four and Six-Legged Robots," *Journal of the Robotics Society of Japan*, vol. 20, no. 3, pp. 237–242, Apr. 2002.

[10] I. Poulakakis, J. Smith, and M. Buchler, "Experimentally validated bounding models for the Scout II quadrupedal robot," in *IEEE International Conference on Robotics and Automation, 2004. Proceedings. ICRA '04. 2004*, vol. 3, Apr. 2004, pp. 2595–2600 Vol.3.

[11] D. Chang, J. Kim, D. Choi, K.-J. Cho, T. Seo, and J. Kim, "Design of a slider-crank leg mechanism for mobile hopping robotic platforms," *Journal of Mechanical Science and Technology*, vol. 27, no. 1, pp. 207–214, Jan. 2013.

[12] J. D. Hauenstein and S. N. Sherman, "Using Monodromy to Statistically Estimate the Number of Solutions," *Springer's Proceedings in Advanced Robotics*, 2021.

[13] A. Baskar and M. Plecnik, "Synthesis of Six-bar Timed Curve Generators of Stephenson-type Using Random Monodromy Loops," *Journal of Mechanisms and Robotics*, vol. 13, no. 1, 2020.

[14] A. P. Morgan and A. J. Sommese, "Coefficient-parameter polynomial continuation," *Appl. Math. Comput.*, vol. 29, no. 2, part II, pp. 123–160, 1989.

[15] H. Nolle, "Linkage coupler curve synthesis: A historical review — I. Developments up to 1875," *Mechanism and Machine Theory*, vol. 9, no. 2, pp. 147–168, Jun. 1974.

[16] J. Yao and J. Angeles, "Computation of all optimum dyads in the approximate synthesis of planar linkages for rigid-body guidance," *Mechanism and Machine Theory*, vol. 35, no. 8, pp. 1065–1078, Aug. 2000.

[17] A. J. Sommese and C. W. Wampler, II, *The Numerical Solution of Systems of Polynomials Arising in Engineering and Science*. World Scientific Publishing Co. Pte. Ltd., Hackensack, NJ, 2005.

[18] D. J. Bates, J. D. Hauenstein, A. J. Sommese, and C. W. Wampler, *Numerically solving polynomial systems with Bertini*, ser. Software, Environments, and Tools. Society for Industrial and Applied Mathematics (SIAM), Philadelphia, PA, 2013, vol. 25.

[19] M. Raghavan and B. Roth, "Solving Polynomial Systems for the Kinematic Analysis and Synthesis of Mechanisms and Robot Manipulators," *Journal of Mechanical Design*, vol. 117, no. B, pp. 71–79, Jun. 1995, publisher: American Society of Mechanical Engineers Digital Collection.

[20] J. Verschelde, "Algorithm 795: Phcpack: A general-purpose solver for polynomial systems by homotopy continuation," *ACM Trans. Math. Softw.*, vol. 25, no. 2, p. 251–276, Jun. 1999.

[21] J. D. Hauenstein, L. Oeding, G. Ottaviani, and A. J. Sommese, "Homotopy techniques for tensor decomposition and perfect identifiability," *Journal fÃ¼r die reine und angewandte Mathematik (Crelles Journal)*, vol. 2019, no. 753, pp. 1–22, 2019. [Online]. Available: https://doi.org/10.1515/crelle-2016-0067

[22] J. D. Hauenstein and J. I. Rodriguez, "Multiprojective witness sets and a trace test," *Advances in Geometry*, vol. 20, no. 3, pp. 297–318, 2020. [Online]. Available: https://doi.org/10.1515/advgeom-2020-0006

[23] D. J. Bates, J. D. Hauenstein, A. J. Sommese, and C. W. Wampler, "Bertini: Software for numerical algebraic geometry," Permanent doi: dx.doi.org/10.7274/R0H41PB5.

[24] T. Duff, "Applications of Monodromy in Solving Polynomial Systems," Ph.D. dissertation, Georgia Institute of Technology, Atlanta, Georgia, USA, Aug. 2021.

[25] D. J. Bates, J. D. Hauenstein, A. J. Sommese, and C. W. Wampler, II, "Adaptive multiprecision path tracking," *SIAM J. Numer. Anal.*, vol. 46, no. 2, pp. 722–746, 2008.

[26] D. J. Bates, J. D. Hauenstein, and A. J. Sommese, "Efficient path tracking methods," *Numer. Algorithms*, vol. 58, no. 4, pp. 451–459, 2011.

[27] D. Brown, "Tracker Video Analysis Software," www.physlets.org/tracker/.